Geochimica et Cosmochimica Acta 350 (2023) 16–27

Contents lists available at ScienceDirect

Geochimica et Cosmochimica Acta

journal homepage: www.elsevier.com/locate/gca

Mass-dependent nickel isotopic variations in achondrites and lunar rocks

Shui-Jiong Wang [a,*], Shi-Jie Li [b], Yangting Lin [c], Si-Zhang Sheng [a]

[a] State Key Laboratory of Geological Processes and Mineral Resources, China University of Geosciences (Beijing), Beijing 100083, China
[b] Center for Lunar and Planetary Sciences, Institute of Geochemistry, Chinese Academy of Sciences, Guiyang, China
[c] Key Laboratory of Earth and Planetary Physics, Institute of Geology and Geophysics, Chinese Academy of Sciences, Beijing, China

ARTICLE INFO

Associate editor: Frederic Moynier

Keywords:
Nickel isotopes
Achondrite
Moon
Late accretion
Giant impact

ABSTRACT

We present high-precision mass-dependent nickel isotopic data for a comprehensive suite of achondrites and lunar rocks, providing key insights into the early planetary differentiation and Earth-Moon system formation. The primitive achondrites display high Ni contents and invariant Ni isotopic compositions. Incomplete core-mantle differentiation in primitive achondrite parent bodies resulted in the retention of metal in the mantle, which dominated the Ni budget and accounted for the bulk chondritic Ni isotopic values. The highly reduced differentiated achondrites, aubrites and an ungrouped achondrite (NWA 8409), have variable, and extremely light Ni isotopic compositions. Acid leaching experiments demonstrate that the sulfides are a significant host of light Ni isotopes in aubrites. The most extreme Ni isotope values of aubrites may be due to large Ni isotope fractionation accompanied by silicate-sulfide-metal separation during differentiation of the parent bodies, and subsequent global disruptive collision and reassembly with variably high proportions of sulfides enriched in the mantle. The howardite-eucrite-diogenite (HED) meteorites show Ni isotopic variations that are positively correlated with Ni/Co ratios, a feature that cannot be produced by igneous differentiation. Late accretion of high-Ni and high-Ni/Co chondritic materials after core formation of their likely parent body, Vesta, could have accounted for this correlation. Thus, the primitive silicate mantle of Vesta may have sub-chondritic Ni isotopic compositions, implying possible Ni isotope fractionation during core-mantle differentiation of small planetary bodies. The lunar breccia meteorites have homogenously chondritic Ni isotope values, together with their high Ni/Co of bulk rock and metals therein, suggesting impact contamination. Lunar basalt meteorites have low Ni/Co ratios and are systematically isotopically lighter than the breccias, displaying a positive correlation between Ni isotope value and Ni/Co ratio, as that seen in the HEDs. Therefore, the Ni isotopic systematics in lunar rocks also indicates the effect of late accretion, with the primitive lunar mantle having sub-chondritic Ni isotope values. This implies that the Moon-forming impactor, Theia, was likely an aubrite-like differentiated planetary body whose mantle was enriched in light Ni isotopes. We suggest that there was significant Ni isotope fractionation between core and mantle during differentiation of early formed small planetary bodies, but this signature can be obscured by late accretion in the bulk achondrite records.

1. Introduction

Early planetary accretion and differentiation processes recorded in meteorites provide complementary information to our understanding of the formation and evolution of the large, rocky planets (e.g., Day, 2015). Metal-silicate separation during partial melting of planetary bodies caused quantitative segregation of siderophile (metal-loving) elements into the metal phase, potentially accompanied by mass-dependent isotope fractionations (Bourdon et al., 2018; Creech et al., 2017a, 2017b; Hopp and Kleine, 2021; Wang et al., 2014a). Nickel is the second most abundant siderophile element in the Solar System. Mass-dependent isotopic compositions of Ni (expressed as $\delta^{60/58}$Ni, the per mil deviation of ^{60}Ni/^{58}Ni ratios relative to SRM986 standard) in different types of chondrite meteorites fall in a limited range of $+0.23 \pm 0.11$‰ (2SD) (Cameron et al., 2009; Chernonozhkin et al., 2016; Gall et al., 2017; Gueguen et al., 2013; Klaver et al., 2020; Steele et al., 2011; Wang et al., 2021). Iron meteorites, which represent Fe-Ni samples from the cores of asteroids and planetesimals, have $\delta^{60/58}$Ni values within this 'chondritic' range (see compiled in Wang et al. 2021), which is predictable from a mass-balance perspective because >90% of Ni budget is located

* Corresponding author.
E-mail address: wsj@cugb.edu.cn (S.-J. Wang).

https://doi.org/10.1016/j.gca.2023.04.004
Received 9 December 2022; Accepted 4 April 2023
Available online 11 April 2023

in the core during planetary differentiation. The Ni isotopic composition of the silicate mantle of planetary bodies is largely depended on the degree of Ni segregation and isotope fractionation factors during core-mantle differentiation. Experimental and theoretical studies suggest that Ni isotopes hardly fractionate under high-pressure and -temperature conditions applicable to core-mantle differentiation in large planetary bodies, such as Earth (Lazar et al., 2012; Wang et al., 2021; Guignard et al., 2020). For smaller bodies, whether resolvable Ni isotope fractionation existed remains unknown. It can be tested by examining the Ni isotopic systematics in meteorites that represent predominantly silicate materials from asteroids and planets that have partially to fully melted.

Systematic Ni isotopic studies on terrestrial rocks found that the Bulk Silicate Earth (BSE) has an average Ni isotope value (+0.10 ± 0.07‰) slightly lower than the chondrites (Klaver et al., 2020; Wang et al., 2021). The Earth's main accretion stage in the first 30–100 Ma of the Solar System brought to about 85–90% of its current volume (e.g., Kleine et al., 2009; Mezger et al., 2020). If metal and silicate melts equilibrated completely at this high-pressure and -temperature stage, there was a limited Ni isotope fractionation between core and mantle of the proto-Earth (Lazar et al., 2012; Wang et al., 2021; Guignard et al., 2020). Wang et al. (2021) proposed that the difference in Ni isotopes between the BSE and chondrites was established during Earth's late-accretion stages, probably through the Moon-forming giant impact which contributed >20% of the Ni budget of the BSE (Rubie et al., 2011). That is, the impactor, Theia, may be an important source of light Ni isotopes to the Earth's mantle through a core-merging giant impact (Rubie et al., 2011; Zhou et al., 2022). It is thought that Theia was likely a differentiated, Mars-sized planetary body whose mantle is enriched in light Ni isotopes (Wang et al., 2021). This hints a possibility that early planetary melting and chemical differentiation may have produced significant Ni isotope fractionations. However, the hypothesis was solely built upon the comparative Ni isotopic study of between Earth and chondrites. To further test the veracity, Ni isotopic data of lunar rocks and achondrites that record different degrees of differentiation on distinct planetary bodies in the early Solar System are needed.

Unfortunately, there is scant information on Ni isotopic variations in achondrites and lunar rocks. Chernonozhkin et al. (2016) reported Ni isotopic data for the silicate and metal fractions in pallasites and mesosiderites. The $\delta^{60/58}$Ni values of the silicate fraction in four pallasites vary widely from +0.55‰ to +1.22‰, likely resulting from diffusion-controlled kinetic isotope fractionation against the metal fraction (from −0.81‰ to +0.45‰) during later cooling stages, rather than a pristine record of mantle-core differentiation (Chernonozhkin et al., 2016). The silicate fractions from two mesosiderites have $\delta^{60/58}$Ni of −0.15‰ and +0.02‰, respectively, whereas the metal fractions in mesosiderites have an average $\delta^{60/58}$Ni of +0.18 ± 0.02‰. Recently, Zhu et al. (2022) reported an average $\delta^{60/58}$Ni value of +0.26 ± 0.13‰ for 22 ureilites. The value is consistent with that of chondrites and that of iron meteorites (see compiled by Wang et al., 2021), suggesting that high-temperature core-mantle differentiation in the ureilite planetary body (UPB) does not significantly fractionate Ni isotopes (Zhu et al., 2022). However, Ni isotopic data of lunar rocks and other types of achondrites are still lacking.

Here, we apply Ni isotopic analysis to a comprehensive set of achondrites, with estimated oxygen fugacity (f_{O2}) from high to low ($\Delta IW = +1 \sim -6$) (e.g., Righter et al., 2016), ranging from angrites, brachinites, howardite-eucrite-diogenite (HED) meteorites, ureilites, lodranites, to aubrites and an ungrouped achondrite (NWA 8409). We also measured Ni isotopic compositions of ten lunar meteorites including six feldspathic breccias and four basaltic rocks. These data, combined with newly analyzed trace element abundance data of Ni and Co, are used to evaluate the Ni isotopic behavior during planetesimal differentiation and late accretion, and to place constraints on the nature of the Moon-forming impactor.

2. Samples and analytical methods

2.1. Sample description

All studied samples are meteorites. Achondrite samples selected for this study include four primitive achondrites (two lodranites and two brachinites) and 13 differentiated achondrites (four ureilites, one angrite, three diogenites, one howardite, one eucrite, two aubrites, and one ungrouped achondrite). Lunar meteorite samples include six highland feldspathic breccias, two mare basalts and two gabbros. The majority of samples in this study are "finds". The remaining four observed as "falls" include one diogenite (Tatahouine), one howardite (Saricicek) and two aubrites (Pena Blanca Spring and Norton County).

Primitive achondrites are melting residues that have lost partial silicate and metallic or sulfide-rich melts to varying degrees (Day, 2015; Mittlefehldt et al., 2018; Weisberg et al., 2006). Among the four primitive achondrites studied in this work, the lodranites have experienced some of the least apparent metal and silicate melt-loss, with evidence for silicate melting and high Fe-Ni abundances (Dhaliwal et al., 2017; Keil and McCoy, 2018; McCoy et al., 2006). Two lodranites studied here (NWA 8118 and NWA 6685) are coarse grained consisting of olivine and orthopyroxene in various proportions, with troilite and Fe-Ni metal as accessory minerals (Li et al., 2018). The brachinites represent residues of moderate degrees (<30%) of partial melting of primitive chondritic sources (Day et al., 2012a; Goodrich, 1992; Keil, 2014; Mittlefehldt et al., 2003). The two studied brachinites (NWA 12573 and Kumtag 061) are mainly composed of olivine and pyroxene, with plagioclase, troilite and Fe-Ni metal as accessory minerals.

Differentiated achondrites sample the silicate portion of differentiated planetary bodies, with distinct chemical compositions that are fractionated from chondritic materials (e.g., Day, 2015; Mittlefehldt et al., 2018). Ureilites exhibit some characteristics of both primitive and differentiated achondrites. Because of their silicate mineralogy that requires a high-degree melting and igneous origin, we consider them as differentiated achondrites in this study following Mittlefehldt (2014) and Krott et al. (2014). The four ureilite (NWA 11641, NWA 14282, NWA 6056, and NWA 14281) have a cumulate texture composed of coarse-grained olivine and pyroxene with minor graphitic carbon, troilite and Fe-Ni metal. Angrites are thought to be partial melts of a differentiated asteroidal source formed at the dawn of the Solar System (e.g., Keil, 2012). The studied angrite meteorite (NWA 12934) show a diabasic texture consisting of irregular plagioclase, olivine and pyroxene, with minor amount of Fe-Ni metal, troilite and Mg-Fe spinel. HEDs are considered to originate from asteroid 4 Vesta, with diogenites representing lower crustal or mantle materials, eucrites representing upper crustal materials, and howardites being polymict breccias composed of eucrites and diogenites (Mittlefehldt, 2015). Three diogenites (NWA 8119, NWA 7831, and Tatahouine) are dominated by orthopyroxene with accessory clinopyroxene, olivine, chromite, troilite and metal. Tatahouine is unbrecciated displaying a wellpreserved cumulative texture whereas other diogenites are fragmental breccias. The eucrite (Camel Donga) contains angular grains of pyroxene and calcic plagioclase as the main silicate phases, and metallic iron up to 2 wt%. The howardite (Saricicek) is a breccia consisting of lithic and mineral clasts of eucritic composition in a fine-grained matrix of crushed materials. Aubrites are highly reduced pyroxenitic achondrites that are thought to represent the differentiated products of enstatite chondrite-like parent bodies (Keil, 2010). The Pena Blanca Spring aubrite is a fragmental breccia consisting of enstatite with sulfide and metal as accessory minerals. The Norton County aubrite is a fragmental impact breccia consisting of coarse and angular enstatite crystal fragments, embedded into a clastic matrix, with higher troilite and metal contents (Wilbur et al., 2022). It has been suggested that the metal in the Norton County aubrite represents a fraction of the metallic Fe-Ni that was not completely segregated from the silicates during partial melting of an enstatite chondrite-like precursor lithology (Casanova et al., 1993). The

ungrouped achondrite NWA 8409, consists of calcic plagioclase, diopside and forsterite with accessory Cr-bearing troilite and kamacite. It has petrological and geochemical characteristics that are distinct from those of all other known achondrites, and likely represents a crustal rock from an extensively differentiated parent body (Barrat et al., 2015; Goodrich et al., 2017).

Five of six lunar breccia meteorites in this study (NWA 11474, NWA 11266, NWA 11273, Lahmada 020, and DaG 400) are feldspathic breccias composed of mineral clasts of anorthite, olivine, pyroxene, spinel, troilite and Fe-Ni metal in a finer grained matrix containing small vesicles. The other lunar breccia meteorite (NWA 10203) is a polymict breccia containing at least four distinct lithologies: unbrecciated olivine gabbro, fragmental anorthositic gabbro breccia, fragmental gabbroic breccia, and shock melt veins and pools. Fe-Ni metal and troilite are observed in the fragmental breccias. Lunar meteorite NWA 4734 is a medium- to coarse-grained, subophitic-texture mare basalt consisting of pyroxene and plagioclase with minor olivine as well as other accessary minerals. Lunar mare basalt NWA 14137 is mainly composed of igneous-zoned olivine and pyroxene. Maskelynite makes up approximately 25% of the modal mineralogy. Lunar meteorite NWA 8127 is an olivine gabbro consisting of small grains of olivine, Ti-bearing chromite and ilmenite, poikilitically enclosed in clinopyroxene, with interstitial anorthositic plagioclase. Another lunar olivine gabbro (NWA 6950) is relatively coarse grained with a cumulate igneous texture. The rock is dominated by olivine, low-Ca pyroxene, pigeonite, and subcalcic augite, with interstitial very calcic plagioclase. Troilite and metal occur as accessory minerals.

2.2. Methods

Samples were cut using a diamond wire saw. Following the wire sawing, the saw fines were removed from the cut surface with a fine sandpaper and air duster. Rock chips of roughly 500–1000 mg were further cleaned in MQ water in an ultrasonic bath, after which the leaching solutions were discarded and the residues were washed, dried, and crushed to fine powders in an agate mortar. We suggest this is a must step especially for Ni isotopic analyses because the diamond-coated wire has a nickel-plated or stainless steel core that has extremely high Ni abundances (Supplementary Fig. S1). If used unproperly or corroded, the wire cut could lead to considerable Ni contamination, and unfortunately meaningless data. Around 20–200 mg sample powders were digested using a mixture of concentrated HF-HNO_3 (2:1) followed by *Aqua regia* (HCl:HNO_3 = 3:1) in 15 ml Teflon beakers to ensure complete dissolution without any visible particles. In addition to bulk-rock dissolution, the non-magnetic fractions of two aubrites were subjected to acid leaching. The non-magnetic fractions were firstly separated with a hand-magnet from fine grained bulk-rock powders, and were then placed in 4 ml of cold 3 M HCl for 6 h to separate the sulfide and silicate fraction following Luck et al. (2005) and Moynier et al. (2011). We acknowledge that this separation procedure is not perfect because (1) metals can be attached to the non-magnetic fraction (Torigoye and Shima, 1993), (2) the leachate can contain a minor dissolved metal fraction, and (3) possible kinetic isotope fractionation during acid leaching cannot be excluded. The leachates (presumably sulfide fraction) were dissolved in 6 M HCl, and the residues (presumably silicate fraction) were decomposed using the same procedure as bulk-rock powders. After complete dissolution, samples were dried and 3% HNO_3 was added in preparation for trace element analyses.

Trace elements analyses of Ni and Co were conducted using a Thermo Element XR inductively coupled plasma-mass spectroscopy (ICP-MS) system in medium resolution mode at China University of Geosciences, Beijing. Aliquots of samples dissolved in 3% HNO_3 were diluted by weight with appropriate dilution factors of 5000–20000. Nine standard solutions were made from a multi-element ICP standard solution to reach Ni and Co concentrations ranging from 0.51 to 495.78 ng/g, which cover the concentrations of these elements in sample solutions. These standard solutions together with the blank were used to establish the calibration curve to determine the elemental concentrations of samples. A 20 ng/g pure In solution was used as an internal standard to correct for potential drift during ICPMS analysis. Solutions of reference materials including a carbonaceous chondrite (Allende), four terrestrial igneous rocks (BHVO-2, BIR-1, GSR-1, and JG-1) and a manganese nodule (Nod-P-1) were used as external standards and analyzed together with samples for evaluating the precision and the accuracy of the data. The data agree well with literature data within ±5% and are reported in Supplementary Fig. S2. We also measured Fe/Ni ratio of our samples, and the data of reference materials agree well with literature data (Supplementary Fig. S3).

Nickel was purified at the Isotope Geochemistry Laboratory of the China University of Geosciences, Beijing. Based on the measured Ni concentration obtained on the Thermo Element XR ICP-MS, aliquots of sample solutions containing 800 ng Ni were spiked with a ^{61}Ni–^{62}Ni double spike to reach an optimal spike: sample ratio of 60:40. The mixtures were refluxed on a hotplate to ensure sample–spike equilibration before column chemistry. Separation of Ni from matrices was achieved using a three-stage, chromatography procedure (Spivak-Birndorf et al., 2018; Wang et al., 2019; Wang et al., 2021). Briefly, the first column uses anion exchange resin Bio-Rad AG1W-X8 to separate Ni from Fe and other matrix elements. The second column applies a mixture of 15 vol% 10 M HCl and 85 vol% acetic acid using cation exchange resin Bio-Rad AG50W-X8 to separate Ni from elements such as Mg, Al, Ca and Ti. The last column uses the anion exchange resin Bio-Rad AG1W-X8 to further purify Ni by 100% acetic acid to remove Mn and alkali elements. The total procedural blank contains <3 ng Ni, which is negligible compared to ~800 ng Ni from samples that was processed through the column.

Nickel isotopic data were determined on a Thermo Scientific® Neptune Plus multi-collector inductively coupled plasma mass spectrometer in medium resolution mode with an Aridus II introduction system. Four Ni isotopes (^{62}Ni, ^{61}Ni, ^{60}Ni, ^{58}Ni) together with ^{57}Fe were measured simultaneously on separate Faraday cups (H2, H1, Axial, L1 and L3). The measurement of ^{57}Fe was used to correct for a potential interference from ^{58}Fe on ^{58}Ni. In blank solution, there are no detectable peaks for polyatomic interferences such like $^{40}Ar^{18}O^+$ and $^{40}Ar^{17}OH^+$ on mass 58. The background Ni signal for ^{60}Ni was $<10^{-3}$ V, which is negligible compared to the sample signals of ~7–8 V (100 ng/g solution). Samples were bracketed with measurements of a double-spiked NIST SRM 986 at a similar concentration. The double-spike equations, which assume that sample and reference material lie on the same exponential law fractionation line, were then applied to correct for isotope fractionation caused by instrument-induced mass bias and imperfect column yields. The Ni isotopic ratio is presented in the delta (δ) notation as per mil deviation (‰) relative to SRM 986:

$$\delta^{60/58}Ni = [(^{60}Ni/^{58}Ni)_{sample}/(^{60}Ni/^{58}Ni)_{SRM\ 986} - 1] \times 1000.$$

The precision and accuracy of the analyses were assessed by repeated analysis of two in-house pure Ni solutions (WSJ-1 and WSJ-2), and three rock reference materials (Allende, BHVO-2 and BIR-1) that were processed together with samples. The WSJ-1 and WSJ-2, based on four repeat runs in each analytical session, give $\delta^{60/58}Ni$ of −0.541 ± 0.008‰ (2SD) and +0.306 ± 0.048‰ (2SD), respectively, consistent with our two-year monitor of the two Ni solutions (-0.533 ± 0.037‰ and +0.315 ± 0.049‰). The rock reference materials yield $\delta^{60/58}Ni$ values of +0.250 ± 0.020‰ (n = 4; 2SD) for Allende, +0.064 ± 0.030‰ (n = 4; 2SD) for BHVO-2, and +0.145 ± 0.048‰ (n = 5; 2SD) for BIR-1, in agreement with literature data (Beunon et al., 2020; Chernonozhkin et al., 2015; Gall et al., 2017; Gueguen et al., 2013; Klaver et al., 2020). The long-term precision during the course of this study, based on replicated analyses of the reference materials, was better than 0.05‰ (2SD) on the $^{60}Ni/^{58}Ni$ ratio. Each sample solution was measured at least three times in different analytical sequences on different days, and the

average value was reported together with 2SD.

Our previous study on meteorite samples documented that the presence of nucleosynthetic Ni isotopic anomalous (in ε notation) leads to a slightly biased α-value for double-spike calculation, but does not have a large impact on the mass-dependent Ni isotopic results (Render et al., 2018). Correction of mass-dependent Ni isotope fractionation for non-terrestrial mass-independent isotopic compositions results in uncertainty of ≦0.02‰ (Render et al., 2018), which is small compared to the analytical uncertainty and the magnitude of isotope fractionation seen in our samples. Cosmogenic effects may have affected calculated mass-dependent Ni isotopic compositions of meteorites. Cook et al. (2020) presented theoretical modeling and Ni isotopic measurement to iron meteorites that span a range of exposure histories and found that cosmogenic effects on Ni isotopic ratios are smaller than the current analytical resolution of the Ni isotopic measurement. Saunders (2018) suggested limited cosmogenic effects on the mass-dependent Ni isotopic compositions of lunar samples due to the lack of correlation with the exposure ages of the samples. Finally, the presence of ^{60}Fe and its decay would lead to excess ^{60}Ni in meteorites which have extremely high Fe/Ni ratios. For example, Tang and Dauphas (2012) found high $\varepsilon^{60/58}$Ni (normalized to ^{61}Ni/^{58}Ni) up to 7.09 in meteorites that have anomalously high ^{56}Fe/^{58}Ni ratio of 82591, but those with ^{56}Fe/^{58}Ni ratio < 15000 usually have $\varepsilon^{60/58}$Ni < 1.00. Our samples have low ^{56}Fe/^{58}Ni ratio < 15000 (Table. 1; Supplementary Fig. S4), leading to the impact of decay of ^{60}Fe on ^{60}Ni negligible. Applying our measured ^{56}Fe/^{58}Ni to the regression determined by Tang and Dauphas (2012) yields ^{60}Fe decay-induced $\delta^{60/58}$Ni variation generally lower than 0.06‰, within the analytical uncertainties (Supplementary Fig. S4).

3. Results

Nickel isotopic data of lunar meteorites, primitive and differentiated achondrites, together with Ni and Co contents, are presented in Table 1.

Primitive achondrites have $\delta^{60/58}$Ni varying in a limited range (Fig. 1). Two lodranites (NWA 8118 and NWA 6685) have $\delta^{60/58}$Ni values of +0.237 ± 0.058‰ and +0.081 ± 0.021‰, respectively. Two brachinites (Kumtag 061 and NWA 12573) have $\delta^{60/58}$Ni values of +0.117 ± 0.031‰ and +0.162 ± 0.070‰, respectively. The primitive achondrites have high Ni and Co contents, ranging from 2019 μg/g to 15,646 μg/g and from 297 μg/g to 996 μg/g, respectively (Table 1; Fig. 2), with Ni/Co ratios varying from 6.8 to 20.4, slightly lower than the chondritic value (~20) (Campbell and Humayun, 2003; McDonough and Sun, 1995; Ringwood and Seifert, 1986).

By contrast, differentiated achondrites show large magnitude of Ni isotopic variations (Fig. 1). Four ureilites have relatively homogeneous $\delta^{60/58}$Ni values varying from +0.157 ± 0.029‰ to +0.270 ± 0.030‰, with the average of +0.224 ± 0.097‰. The angrite (NWA 12934) has a $\delta^{60/58}$Ni value of +0.138 ± 0.027‰. The five HED meteorites show larger Ni isotopic variations, with $\delta^{60/58}$Ni value ranging from −0.522 ± 0.033‰ to +0.107 ± 0.050‰ for diogenites (NWA 8119, NWA 7831, and Tatahouine), −0.049 ± 0.055‰ for a eucrite (Camel Donga), and +0.244 ± 0.029‰ for a howardite (Saricicek). Two fragments of Pena Blanca Spring aubrite were studied. One was for bulk-rock analyses and one was subjected to phase separation. The Pena Blanca Spring aubrite has a bulk-$\delta^{60/58}$Ni value of −0.888 ± 0.039‰. The leachate and residue of the non-magnet fraction have $\delta^{60/58}$Ni values of −1.066 ± 0.025‰ and +0.090 ± 0.030‰, respectively. Three different fragments of Norton County aubrite (#2–4) were analyzed for bulk Ni isotopic compositions and one additional fragment (#1) was subject to phase separation. The bulk $\delta^{60/58}$Ni values are relatively homogenous ranging from +0.055 ± 0.036‰ to +0.156 ± 0.044‰, with the average of +0.106 ± 0.101‰. The leachate and residue fractions of Norton County aubrite have $\delta^{60/58}$Ni values of −0.081 ± 0.047‰ and +0.170 ± 0.012‰, respectively (Fig. 1). Two fragments of the highly reduced ungrouped achondrite (NWA 8409) have similar $\delta^{60/58}$Ni values of −1.688 ± 0.023‰ and −1.585 ± 0.045‰, the lowest among all studied achondrites. Among the differentiated achondrites, ureilite and angrite have relatively high Ni (1373–4276 μg/g) and Co contents (81–394 μg/g), with high Ni/Co ratios ranging from 10.9 to 23.5. Other differentiated achondrites have lower Ni content of 13.5–494 μg/g, and Co content of 2.2–130 μg/g. Different fragments of two aubrites have high Ni/Co ratio of 21.4–35.9, while the remaining has Ni/Co ratios in the range of 0.8–9.4.

The six lunar feldspathic breccia meteorites have remarkably homogeneous Ni isotopic compositions, with the average $\delta^{60/58}$Ni of +0.292 ± 0.083‰, falling within the chondritic range (Fig. 1). They have Ni ranging from 96.2 μg /g to 222 μg/g, and Co ranging from 11.9 μg/g to 22.0 μg/g (Table 1; Fig. 2), with high Ni/Co of 6.7–12.1. The four lunar basalt meteorites yield $\delta^{60/58}$Ni values of +0.023 ± 0.042‰ (for NWA 14137), +0.095 ± 0.035‰ (for NWA 4734), +0.168 ± 0.011‰ (for NWA 8127), and +0.228 ± 0.030‰ (for NWA 6950). They have Ni of 27.9–182 μg/g and Co of 32.4–79.6 μg/g (Table 1; Fig. 2), with lower Ni/Co of 0.9–2.4 compared to the lunar breccias.

4. Discussion

Different achondrites provide a record of early planetary melting and chemical differentiation on the Solar System bodies (Day, 2015). The primitive achondrites were derived from the residual mantles of incompletely differentiated planetesimals, and record the local silicate-metal-sulfide segregation and migration at the earliest stage of planetesimal differentiation (Day et al., 2012a; Dhaliwal et al., 2017; Keil and McCoy, 2018; McCoy et al., 2006). The differentiated achondrites are more evolved by large degree of melting and crystallization, and represent the crust and mantle rocks of differentiated parent bodies. They bear information on metal-silicate equilibration during core formation, silicate mantle partial melting and late-accretion additions (Dale et al., 2012; Day et al., 2012b; Wang et al., 2014b). Below, we first evaluate the Ni isotopic variations in primitive and differentiated achondrites to explore the heterogeneity of Ni isotopes in the Solar System, and then discuss the origin of Ni isotopic variations observed in lunar meteorites.

4.1. Nickel isotopic variations in primitive achondrites

Primitive achondrites record low (e.g., lodranite, <20%) to moderate (brachinites, 10–30%) partial melting of their parent bodies, and successive metal-silicate melt segregation or migration (Day, 2015; Mittlefehldt et al., 2018; Weisberg et al., 2006). For instance, lodranites are thought to be residues that have lost small amount of silicate and Fe-Ni-S melts, whereas the brachinites seem to have lost larger fractions of these melts (Day et al., 2012a; Dhaliwal et al., 2017; Keil and McCoy, 2018; McCoy et al., 2006). The highly siderophile elements (HSEs) and their isotopic systematics can be fractionated associated with Fe-Ni-S melt extraction and redistribution in the partially-melted achondrites (Creech et al., 2017a, 2017b; Day et al., 2012a; Dhaliwal et al., 2017; Hopp and Kleine, 2021; Horstmann et al., 2014; Rankenburg et al., 2008; Wang et al., 2014a). The moderate siderophile nature of Ni makes isotope fractionation of Ni possible by these processes.

The direction and magnitude of equilibrium Ni isotope fractionations during planetary metal-silicate-sulfide differentiation have been experimentally and theoretically examined (Fig. 3). Lazar et al. (2012) presented three-isotope experiments to determine the equilibrium Ni isotope fractionation between solid metal and talc [$Ni_3Si_4O_{10}(OH)_2$] (as a representative of silicate). Although talc does not simply represent the bulk composition of the planetary silicate melts or mantle, nor did the experimental temperature approach 1000 °C (from 500 °C to 900 °C), the results predict an equilibrium temperature-fractionation relationship of $\Delta^{62/58}Ni_{metal\text{-}silicate} = 0.25(\pm0.02) \times 10^6/T^2$, that is <0.02‰ in terms of $\Delta^{60/58}Ni_{metal\text{-}silicate}$ under Earth's core-formation condition (>2500 K). Guignard et al. (2020) 's experiments on diffusion of Ni from a pure nickel wire to silicate melts confirmed the enrichment of heavy Ni

Table 1
Nickel isotopic compositions, Co and Ni contents, and Fe/Ni of achondrites, lunar meteorites and reference materials.

Meteorite	Classification	Type	$\delta^{60/58}$Ni (‰)	2sd	n	Co (ug/g)	Ni (ug/g)	Ni/Co	Fe/Ni
Lunar rocks									
NWA 11474	Lunar feldspathic breccia	find	0.362	0.083	3	22.0	222	10.1	147
	Replicate		0.356	0.002	3				
	Ave.		0.359	0.009					
NWA 11266	Lunar feldspathic breccia	find	0.309	0.026	3	14.2	97.9	6.9	295
NWA 10203	Lunar polymict breccia	find	0.317	0.001	3	12.6	150	12.0	160
	Replicate		0.298	0.033	3				
	Ave.		0.308	0.027					
NWA 11273	Lunar feldspathic breccia	find	0.249	0.067	3	17.7	138	7.8	217
Lahmada 020	Lunar feldspathic breccia	find	0.254	0.054	3	14.4	96.2	6.7	282
DAG 400	Lunar anorthositic breccia	find	0.277	0.091	3	11.9	144	12.1	159
NWA 4734	mare basalt	find	0.107	0.057	3	32.4	27.9	0.9	4985
	Replicate		0.082	0.076	3				
	Ave.		0.095	0.035					
NWA8127	olivine gabbro	find	0.168	0.011	3	79.6	174	2.2	765
NWA6950	olivine gabbro	find	0.228	0.030	3	75.1	182	2.4	689
NWA14137	Lunar mare basalt	find	0.023	0.042	3	34.2	29.5	0.9	4910
Primitive achondrites									
NWA 8118	Lodranite	find	0.237	0.058	3	996	15,646	15.7	12
NWA 6685	Lodranite	find	0.081	0.021	3	390	6337	16.2	22
Kumtag 061	Brachinite	find	0.117	0.031	3	297	2019	6.8	101
NWA12573	Brachinite	find	0.162	0.070	3	495	10,089	20.4	19
Differentiated achondrites									
NWA 11641	Ureilite	find	0.216	0.034	3	394	4276	10.9	33
	Replicate		0.235	0.034	3				
	Ave.		0.226	0.026					
NWA 14282	Ureilite	find	0.157	0.029	3	81.0	1904	23.5	58
NWA 6056	Ureilite	find	0.270	0.030	3	123	1373	11.1	67
NWA14281	Ureilite	find	0.245	0.050	3	170	1990	11.7	51
NWA 12934	Angrite	find	0.128	0.070	3	228	3689	16.2	45
	Replicate		0.147	0.040	3				
	Ave.		0.138	0.027					
NWA 8119	Diogenite	find	−0.522	0.033	4	37.4	29.7	0.8	3683
NWA 7831	Diogenite	find	0.107	0.050	3	130	494	3.8	254
Tatahouine	Diogenite unbrecciated	fall	−0.177	0.012	3	14.3	13.5	0.9	7649
	Replicate		−0.203	0.042	3				
	Ave.		−0.190	0.036					
Saricicek	Howardite	fall	0.244	0.029	3	24.2	227	9.4	525
Camel Donga	Eucrite	find	−0.029	0.061	3	5.02	31.4	6.3	4231
	Replicate		−0.068	0.030	3				
	Ave.		−0.049	0.055					
Pena blanca spring	Aubrite	fall	−0.880	0.066	3	2.20	79.0	35.9	237
	Replicate		−0.910	0.043	3				
	Replicate		−0.874	0.020	3				
	Ave.		−0.888	0.039					
	non-magnetic leachate		−1.066	0.025	4				
	non-magnetic residue		0.090	0.030	3				
Norton County	Aubrite	fall	0.071	0.026	3	11.0	362	32.9	24
	Replicate		0.036	0.021	3				
	Replicate		0.060	0.030	3				
	Ave.		0.055	0.036					
	Duplicate		0.156	0.044	3	7.65	164	21.4	33
	Duplicate		0.106	0.040	3	3.83	90.0	23.5	53
	Non-magnetic leachate		−0.081	0.047	3				
	Non-magnetic residue		0.170	0.012	3				
NWA 8409	Achondrite-ung	find	−1.680	0.056	3	18.8	72.4	3.9	104
	Replicate		−1.696	0.053	3				
	Ave.		−1.688	0.023					
	Duplicate		−1.585	0.045		14.0	53.4	3.8	159
Reference materials									
Allende	Carbonaceous chondrite		0.250	0.020	4	620	15,069	24.3	13
BHVO-2	Hawaiian basalt		0.064	0.030	4	41.7	109	2.6	638
BIR-1	Icelandic basalt		0.145	0.048	5	52.0	174	3.3	
GSR-1	Granite					2.6	1.3	0.5	9895
JG-1	Granodiorite					3.4	6.2	1.9	2218
NOD-P-1	Mn Nodule					2201	13,481	6.1	3.6

Replicate: repeat column chemistry and instrumental analysis from the same sample solution.
Duplicate: repeat sample dissolution, column chemistry and instrumental analysis.

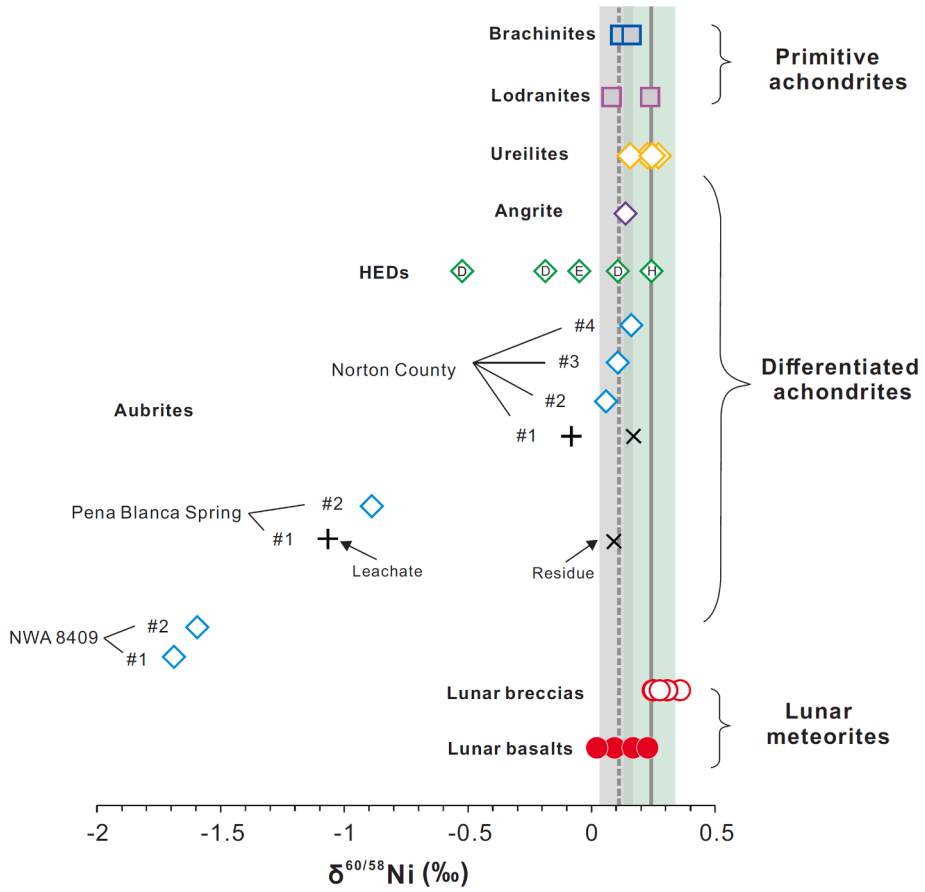

Fig. 1. Mass-dependent Ni isotopic compositions of achondrites and lunar meteorites. The solid and dashed bars represent the average Ni isotopic compositions of chondrites and Bulk Silicate Earth (BSE), respectively. Those of the leachate (+) and residue (x) from acid leaching of the non-magnetic fraction of aubrites are also shown.

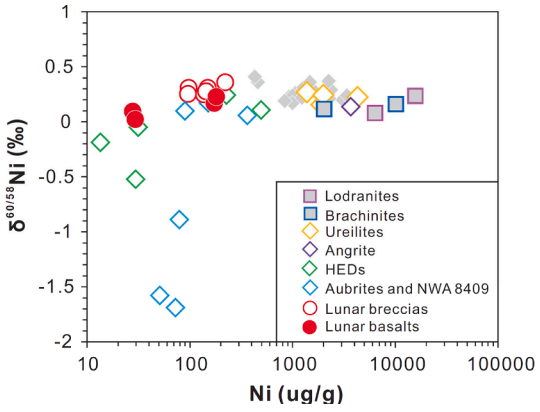

Fig. 2. Nickel isotopic compositions *versus* the Ni contents for all investigated achondrites and lunar meteorites. Literature data of ureilites (small grey diamond) are from Zhu et al. (2022).

isotopes in the metal fraction with a very small equilibrium Ni isotope fractionation of 0.02 ± 0.04‰ at 1623 K. Wang et al. (2021) employed first-principle calculations on the Ni isotope fractionation between silicate minerals/melts and Fe-Ni-(S) melts at high pressures up to 60 GPa. They found that the S-free Ni-Fe alloy is slightly enriched in heavy Ni isotopes relative to the silicate ($\Delta^{60/58}Ni_{metal\text{-}silicate}$ = 0.005‰ at T = 2500 K), whereas the S-rich Ni-Fe alloy is slightly enriched in light isotopes ($\Delta^{60/58}Ni_{metal\text{-}silicate}$ = −0.01‰ at T = 2500 K). Overall, high-temperature equilibrium Ni isotope fractionation between

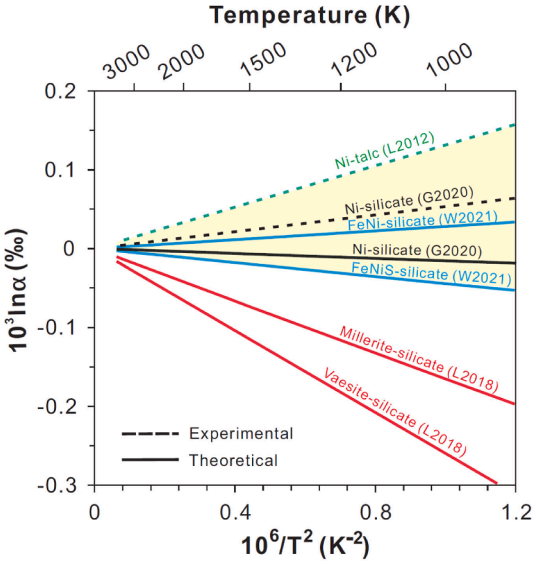

Fig. 3. Equilibrium Ni isotope fractionation factor between metal, silicate, and sulfide. Ni-Talc (L2012) from Lazer et al. (2012); Ni-silicate (G2020) from Guignard et al. (2020); FeNi(S)-silicate from Wang et al., (2021). The Ni isotope fractionations between sulfide (millerite and vaesite) and silicate (L2018) are calculated from Liu et al., (2018) and Wang et al., (2021).

Fe-Ni-(S) melt and silicate melts is small. We apply these isotope fractionation factors to a core-forming mass balance model by assuming complete metal-silicate segregation and full equilibrium during planetary differentiation.

Nickel is siderophile, and thus is quantitively segregated into the metal phase during core formation. The metal/silicate partition coefficient of Ni ($D^{Ni}_{metal\text{-}silicate}$) is strongly correlated to pressure and to oxygen fugacity (f_{O2}), increasing over three orders of magnitude with decreasing pressure (from 100 GPa to 1 bar) and f_{O2} (from IW to IW-6) (Cartier et al., 2022; Fischer et al., 2015). The fraction of Ni partitioned into the silicate mantle of a planetary body is given by:

$$f = M_{mantle}/(M_{mantle} + D \times M_{core})$$

where M is the mass fraction of mantle or core. The $\delta^{60/58}$Ni value of the silicate mantle can then be calculated using the Rayleigh fractionation equation:

$$\delta^{60/58}Ni_{silicate} = \delta^{60/58}Ni_{PB} + \Delta^{60/58}Ni_{metal-silicate} \times \ln f$$

where the $\Delta^{60/58}Ni_{metal\text{-}silicate}$ is the isotope fractionation factor between metal and silicate, and $\delta^{60/58}Ni_{PB}$ is the Ni isotopic composition of the parent body which is assumed to be chondritic ($\delta^{60/58}$Ni = +0.23‰).

Accordingly, Ni in the planetary core remains chondritic, whereas the Ni in a certain planetary mantle can be isotopically either heavier or lighter relative to the chondritic Ni isotopic composition. The degree of this enrichment or depletion depends on the $\Delta^{60/58}Ni_{metal\text{-}silicate}$ and $D^{Ni}_{metal\text{-}silicate}$, which are combinedly a function of temperature, pressure and f_{O2}. Nevertheless, since the $\Delta^{60/58}Ni_{metal\text{-}silicate}$ at high temperature is too small, the modelling shows that metal-silicate segregation induced Ni isotopic variation in the planetary mantle is generally limited (Fig. 4). In extreme cases where $\Delta^{60/58}Ni_{metal\text{-}silicate}$ is as large as +0.10‰ corresponding to metal-silicate segregation at low temperature of ~1200 K (Fig. 3) and $D^{Ni}_{metal\text{-}silicate}$ is significantly high (>1000), resolvable isotope fractionations between core and mantle can be produced (Fig. 4).

Because metal-silicate melt segregation did not proceed to completion in the parent bodies of primitive achondrites, the above computation only places the upper and lower bounds of the $\delta^{60/58}$Ni value that primitive achondrites can have. The high Ni contents and high Ni/Co of studied samples are consistent with high metal abundances observed in primitive achondrites, which likely controlled the Ni budget (Day, 2015). Consequently, the retention of metal in primitive achondrites can obscure any possible Ni isotope fractionation produced during metal-silicate-sulfide melt segregation processes, and likely explain the observed near-chondritic $\delta^{60/58}$Ni values of the bulk primitive achondrites.

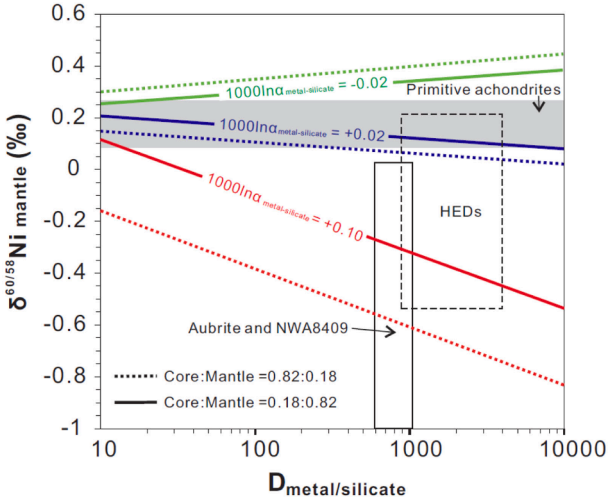

Fig. 4. Mass balance calculation on the Ni isotopic variation in planetary mantle caused by core-mantle differentiation. The mass balance model assumes that the mass ratio between planetary core and mantle ranges from 0.82: 0.18 (dotted) to 0.18: 0.82 (solid), and the isotope fractionation factor $10^3 \ln\alpha_{metal\text{-}silicate}$ in the range of −0.02‰ to +0.10‰. The gray bar represents the range of Ni isotope values of primitive achondrites. The dashed and solid boxes represent the range of HEDs and aubrites (and NWA 8409), respectively. The ranges of $D^{Ni}_{metal/silicate}$ for core-mantle differentiation of Vesta parent body and AUPB are from Cartier et al. (2022).

4.2. Nickel isotopic variations in differentiated achondrites

4.2.1. Origin of Ni isotope fractionation in highly reduced achondrites

The highly reduced aubrites and an ungrouped achondrite (NWA 8409) are the rocks with the most extreme $\delta^{60/58}$Ni values in differentiated achondrites (Fig. 1). The aubrites are generally considered to be samples of the sulfur-rich silicate portion of a differentiated enstatite chondrite-like parent body (Keil, 2010). The Pena Blanca Spring aubrite (with bulk $\delta^{60/58}$Ni = −0.888 ± 0.039‰; [Ni] = 79 μg/g) is one of the least brecciated of all aubrites, containing ~0.48 vol% sulfides plus minor metal (Wilbur et al., 2022). The Norton County aubrite is a fragmental impact breccia, with higher abundance of Fe-Ni metal (~0.85 vol%) and sulfide (~2.3 vol%) (Wilbur et al., 2022). Three fragments of Norton County aubrites yield an average $\delta^{60/58}$Ni value of +0.106 ± 0.101‰. The ungrouped achondrite (NWA 8409), is paired to a more extensively studied NWA 7325 (Archer et al., 2019). These meteorites are cumulate olivine gabbros initially thought to be derived from the planet Mercury, but now is believed to originate from a highly reduced, small parent body unsampled by any other achondrites (Barrat et al., 2015; Goodrich et al., 2017; Koefoed et al., 2016; Yang et al., 2020). Two fragments of the NWA 8409 give an average $\delta^{60/58}$Ni value of −1.637 ± 0.145‰.

We evaluate the role of core formation in the aubrite parent body (AUPB) on the Ni isotopic variations in aubrites. Different types of enstatite chondrites (EH3, EH4, EH5, EL4, and EL6) have a homogeneous $\delta^{60/58}$Ni value of +0.22 ± 0.07‰ (Wang et al., 2021), which we assume to be the initial Ni isotopic composition of the AUPB. Core formation in the AUPB took place at relatively low temperatures of <1600 K (Ray et al., 2021; Righter and Drake, 1997), which would permit to larger metal-silicate Ni isotope fractionations relative to that on Earth. In addition, due to the low differentiation pressure and highly reduced environment (down to IW-6), Ni strongly partitioned into the core of AUPB with a high $D^{Ni}_{metal/silicate}$ of ~850 (Cartier et al., 2022). All these factors would lead to larger Ni isotope fractionation during the core-mantle differentiation of AUPB according to the mass balance model above. However, the $\delta^{60/58}$Ni values of Pena Blanca Spring aubrite and NWA 8409 are too low to be the sole results of metal-silicate segregation (Fig. 4). Other processes must have modified the Ni isotopic systematics.

Igneous differentiation with equilibrium isotope fractionation between silicate minerals and melt is unlikely to explain the abnormally low $\delta^{60/58}$Ni values of the aubrites and NWA 8409. Terrestrial peridotites, komatiites, and oceanic basalts (MgO > 5%) have $\delta^{60/58}$Ni values typically varying in a much smaller range (Gall et al., 2017; Klaver et al., 2020; Saunders et al., 2022; Saunders et al., 2020; Sheng et al., 2022; Wang et al., 2021), suggesting that partial melting of the mantle and fractional crystallization in ultramafic to mafic rocks do not lead to significant Ni isotope fractionations. This is because major mantle silicate minerals such as olivine, orthopyroxene, and clinopyroxene have similar Ni—O coordination environments with nearly identical Ni—O bonding lengths that are comparable to those in the silicate melts (e.g., 2.106 Å for Ni—O in olivine, 2.085 Å for Ni—O in orthopyroxene, and 2.070 Å for Ni—O in clinopyroxene; 1.98–2.06 Å for Ni—O in melts) (Ganguly and Domeneghetti, 1996; Klaver et al., 2022; Lager and Meagher, 1978; White et al., 1971), giving rise to limited Ni isotope fractionation during melting and crystallization of these minerals. Only the sulfide minerals have a longer Ni-S bonding length (e.g., 2.26 to 2.39 Å; Liu et al., 2018) than the Ni—O bonding in silicate minerals, and thus prefer light Ni isotopes (Fig. 3) (Gueguen et al., 2013; Hofmann

et al., 2014; Liu et al., 2018; Wang et al., 2021). Experimental and theoretical calculations predict that the major components of meteorites, silicate, metal, and sulfide, have distinct Ni isotopic compositions at equilibration, with the enrichment of heavy Ni isotopes in the order of metal > silicate > sulfide (Fig. 3). Terrestrial sulfide-rich komatiites have significantly low $\delta^{60/58}$Ni values (down to −1.04‰) that are negatively correlated with the sulfide contents (Gueguen et al., 2013; Hofmann et al., 2014). This hints the potentially important role of sulfides in accounting for the light Ni isotopic signatures in aubrites and NWA 8409.

Sulfides host a significant portion of Ni in aubrites (Wilbur et al., 2022; Yang et al., 2020). Sequential leaching of the non-magnetic fraction of the two aubrites show that the $\delta^{60/58}$Ni values of leachates (presumably the sulfide fraction) are −1.066 ± 0.025‰ for Pena Blanca Spring aubrite and −0.081 ± 0.047‰ for Norton County aubrite, whereas those of the residues (presumably the silicate fraction) are +0.090 ± 0.030‰ and +0.170 ± 0.012‰, respectively. Although the phase-separation protocols above cannot guarantee perfect magnetic and non-magnetic separation nor does the sulfide and silicate separation, and additionally kinetic isotope fractionation during acid leaching cannot be excluded, the isotopic results of such exercise are consistent with natural observation and theoretical prediction that sulfide fraction is isotopically much lighter than the silicate fraction (Gueguen et al., 2013; Hofmann et al., 2014; Liu et al., 2018; Wang et al., 2021). Significant enrichment of light Ni isotopes in sulfides of the aubrites can be achieved via multiple ways. For instance, sulfide-silicate isotopic exchange during igneous differentiation by analogy to the terrestrial Ni-sulfide deposits can produce isotopically light sulfides (Gueguen et al., 2013; Hofmann et al., 2014). Low-temperature sulfidation of metals or silicate by sulfur-rich gas under highly reduced conditions could also be responsible for the enrichment of light Ni isotopes in the sulfides. Alternatively, chemical diffusion of Ni from the Fe-Ni metal (e.g., kamacite) to troilite during cooling can possibly introduce light isotopes to the sulfides. Yet, we are unable to discriminate these processes without a detail in-situ isotopic study on metal, sulfide and silicate fractions. Previous studies of mass-dependent transitional metal isotopes also found extreme values in aubrites, further pointing towards the sulfide effect. Aubrites have lighter isotopic compositions of Zn ($\delta^{66/44}$Zn) (Moynier et al., 2011) and Fe ($\delta^{56/54}$Fe) (Wang et al., 2014b), and heavier isotopic composition of Cr ($\delta^{53/52}$Cr) (Zhu et al., 2021b) compared to the chondritic values, consistent with theoretical calculations and sequential leaching experiments showing that the sulfide fraction is enriched in lighter Zn and Fe isotopes, and heavier Cr isotopes relative to the silicate and metal (Moynier et al., 2011; Moynier et al., 2017; Wang et al., 2014b; Zhu et al., 2021a). Aubrites have the highest sulfur contents (~1 wt%) among all different types of achondrites, which may be a consequence of the high sulfur solubility of the silicate melts following differentiation of the highly reduced AUPB (Namur et al., 2016). Beside troilite, aubrites contain many rare sulfide phases (of typical lithophile elements such as Mg, Ca, Mn, Ti) that were formed under extremely reducing conditions and are distinctive compared to those in other meteorite types (Lin, 2022). While the Ni isotope fractionation between these sulfide phases has not been determined yet, the complexity of sulfide mineralogy and formation mechanism in aubrites would likely lead to highly Ni isotopic heterogeneity among sulfide phases. Although whether the distribution of Ni and other transitional metal isotopes among sulfide, silicate and metal occurred in a manner of equilibrium or kinetic way is currently unknown, the high sulfide abundance in the aubrites provides an important sink of light Ni-Zn-Fe isotopes and heavy Cr isotopes in the mantle of AUPB.

Previous studies suggested that the aubrite parent bodies experienced an extensive postaccretion processing, including core formation, late addition of chondritic materials, and potentially a global disruptive collision and subsequent reassembly to form a “rubble pile” asteroid (Keil et al., 1989; Okada et al., 1988; van Acken et al., 2012). Such mechanical mixing of materials from different areas of the original parent body or from chondritic materials, with varying proportions of sulfides and metals, can possibly explain the large Ni isotopic variations in the studied aubrites. We did not analyze the Ni isotopic composition of metal fractions in the aubrites. However, since Ni is strongly partitioned into the metal during core-mantle differentiation of the highly reduced AUPB, the core-forming mass balance model above predicts that the metal fraction of the AUPB should have a Ni isotope value similar to the chondritic value, whereas the sulfur-rich silicate fraction of the AUPB can be variably isotopically light. The enrichment of Fe-Ni metals in the Norton County aubrite would have dominated the Ni budget (Wilbur et al., 2022), leading the bulk-$\delta^{60/58}$Ni approaching chondritic value. These Fe-Ni metals in Norton County can be from different depths within the AUPB and remixed with the sampled silicate mantle portion or they can be added during late accretion (Ray et al., 2021; van Acken et al., 2012). Nevertheless, we acknowledge that all above hypotheses are not mutually exclusive given the limited dataset. The origin of the abnormally low $\delta^{60/58}$Ni value in highly reduced achondrites is still enigmatic.

We notice that, in a recent study, Zhu et al. (2023) reported very high Ni isotopic values for Norton County and Pena Blanca Spring aubrites, +0.57 ± 0.06‰ and +0.26 ± 0.01‰, respectively. By contrast, none of our bulk-analyses nor phase separation have observed $\delta^{60/58}$Ni values up to +0.57‰. A simple explanation for this discrepancy may be sample-scale heterogeneity, but our four duplicates of Norton County aubrite and two duplicates of NWA 8409 show that these meteorites have relatively homogenous Ni isotopic compositions (Fig. 1). Nevertheless, sample-scale Ni isotopic heterogeneity is still possible given the heterogeneous distribution of μm-sized particles to nodules of sulfides and metals in aubrites which are the main hosts of Ni, and if such high, super-chondritic Ni isotope value is caused by a kinetic isotope fractionation process operated among different phases in aubrites. Future Ni isotopic analyses coupled with detailed mineralogy and geochemistry study on more aubrites are needed to address this issue.

4.2.2. *Origin of the Ni isotope fractionation in HEDs*

The HEDs also display large magnitude of Ni isotopic variations, with no systematical difference between different types of HEDs (Fig. 1). The three orthopyroxenitic diogenites have $\delta^{60/58}$Ni varying from −0.522‰ to +0.107‰, and the basaltic eucrite has a $\delta^{60/58}$Ni of −0.049 ± 0.055‰. The howardite, as a polymict breccia composed of eucrites and diogenites, has a chondritic $\delta^{60/58}$Ni value of +0.244 ± 0.055‰. One prominent feature is that low-Ni/Co samples have generally light Ni isotopic compositions, whereas samples with high Ni/Co ratios have $\delta^{60/58}$Ni approaching the chondritic value (Fig. 5). Crystal fractionation of olivine and pyroxene can slightly change the melts’ Ni/Co ratio, but cannot fractionate Ni isotopes (Sheng et al., 2022). Separation of low-$\delta^{60/58}$Ni sulfides during igneous differentiation would have lowered the Ni/Co ratio and simultaneously shifted the $\delta^{60/58}$Ni to higher values. Therefore, the positive $\delta^{60/58}$Ni – Ni/Co relationship observed for the HEDs requires other explanations.

Previous studies found that the HEDs (mainly eucrites and diogenites) have HSE contents spanning nearly four orders of magnitude with nearly chondritic patterns, a phenomenon that was attributed to late accretion of chondritic materials following a short-lived magma ocean phase (Dale et al., 2012; Day et al., 2012b). This process could have also influenced the moderate siderophile element of Ni. The HEDs have a limited range for Co (3 to 30 μg/g) but a much wider range for Ni (0.1 to 150 μg/g) (Mittlefehldt, 2015). A compilation of Ni and Co concentrations in HEDs suggests that the entire range of Ni/Co can be explained by involvement of as little as 0.5% chondritic materials (Mittlefehldt, 2015). Chondritic materials have high Ni (>1 wt%) and bulk Ni/Co ratio of around 20 (Campbell and Humayun, 2003; McDonough and Sun, 1995; Ringwood and Seifert, 1986), whereas the pristine igneous lithologies in HEDs have several magnitudes lower Ni and Ni/Co ratio of < 2 (Mittlefehldt, 2015). Thus, chondritic additions at any stages after core formation (e.g., late accretion, late-stage post-crystallization

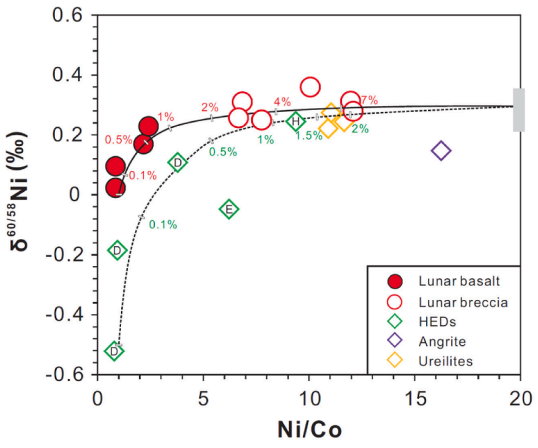

Fig. 5. Variation of $\delta^{60/58}$Ni as a function of Ni/Co in HEDs, lunar rocks, angrite and ureilites. The two curves correspond to mixtures between hypothetical lunar pristine melt (solid) or Vestan pristine melt (dashed) and a chondritic component. The gray box represents the chondritic composition, with [Ni] = 11400 μg/g, [Co] = 505 μg/g, and $\delta^{60/58}$Ni = +0.23‰ (Ringwood and Seifert, 1986; Wang et al., 2021). The hypothetical lunar pristine melt is assumed to have [Ni] = 40 μg/g, [Co] = 40 μg/g, and $\delta^{60/58}$Ni = +0.02‰, while the hypothetical Vestan pristine melt is assumed to have [Ni] = 10 μg/g, [Co] = 10 μg/g, and $\delta^{60/58}$Ni = −0.50‰.

impact liberation and contamination) could elevate the Ni/Co ratio of the HEDs and meanwhile shift the $\delta^{60/58}$Ni towards the chondritic value. The howardite sample (Sariçiçek), which is composed of lithified breccias and solidified melt particles formed by hypervelocity meteoroid impacts on the surface (Unsalan et al., 2019), is likely to contain the impactor component, leading to a high Ni/Co of 9.4 and a chondritic $\delta^{60/58}$Ni value of +0.244 ± 0.029‰ (Fig. 5). The three diogenites (NWA 8119, NWA 7831, and Tatahouine) and a eucrite (Camel Donga), show no clear evidence of either terrestrial or meteoritic contamination (Dale et al., 2012), but they display large Ni isotopic variations from −0.522‰ to +0.107‰. Therefore, it is likely that the positive correlation between $\delta^{60/58}$Ni and Ni/Co ratio resulted from late accretion after planetary core segregation. Late accretion on Vesta parent body may be regional rather than a global effect (Day et al., 2012b), and thus the Ni isotopic heterogeneity may record different magnitude and frequency of late accretion. According to a simple mixing calculation by assuming the diogenite (NWA 8119, $\delta^{60/58}$Ni = −0.522 ± 0.029‰) as the pristine endmember, the estimated proportion of chondritic contributed Ni ranges from 0.1 to 1.5 %. The chondritic $\delta^{60/58}$Ni values, high Ni contents (1373–3689 μg/g), and high Ni/Co ratios (10.9–23.5) of the angrite and ureilites, may suggest that their parent bodies have suffered a similar and universal late accretion event as inferred from the HSEs (Dale et al., 2012).

The above scenario implies that the primitive silicate mantle of Vesta is likely isotopically sub-chondritic, with the $\delta^{60/58}$Ni value located somewhere at −0.50‰ or even lower (Fig. 5). Core-mantle differentiation in Vesta took place at very low pressure and low temperature, with $D^{Ni}_{metal\text{-}silicate}$ well above 2000 (Cartier et al., 2022). Applying metal-silicate isotope fractionation factor ($\Delta^{60/58}Ni_{silicate\text{-}metal}$) of +0.10‰ to the core-forming mass balance model can reasonably produce the $\delta^{60/58}$Ni of the silicate portion as low as −0.50‰ (Fig. 4). Therefore, the data of differentiated achondrites suggest that, core-mantle differentiation on small asteroid parent bodies, because of their large $\Delta^{60/58}Ni_{silicate\text{-}metal}$ and high $D^{Ni}_{metal\text{-}silicate}$, was able to generate significant Ni isotope fractionation. Late accretion on these early formed planetesimals or bodies as a consequence of planetary growth can modify the Ni isotopic systematics of mantle and crustal rocks.

4.3. Nickel isotopic variations in lunar meteorites

A similar picture emerges from the lunar meteorite samples. The high-Ni/Co lunar feldspathic breccias have chondritic $\delta^{60/58}$Ni values whereas the low-Ni/Co lunar basalts have generally lower Ni isotope values, together forming a similar trend as that of HEDs in the $\delta^{60/58}$Ni vs Ni/Co plot (Fig. 5).

There is vast evidence that the brecciated lunar rocks suffered meteoritic contamination (e.g., Day, 2020; Fischer-Gödde and Becker, 2012). The meteoritic materials striking the Moon have high Ni (>1 wt %) and bulk Ni/Co ratio of around 20 (Campbell and Humayun, 2003; McDonough and Sun, 1995; Ringwood and Seifert, 1986), whereas lunar parent melts are thought to have lower Ni (~40–60 ppm) and low Ni/Co ratio of ~1 (Day, 2020). Numerous brecciated Apollo samples and lunar meteorites have high Ni/Co ratios approaching the chondritic value for the bulk rock and metal grains therein, indicating the presence of exogenous meteoritic materials (Day, 2020). The studied lunar breccia meteorites have high bulk-rock Ni/Co ratios (6.1–12.1), and metal grains from selected breccia samples also show high Ni/Co of 11.8–14.1 (Supplementary Fig. S5), indicating potential impact contamination. Although the six breccia samples contain varying proportions of dominantly anorthite, olivine and pyroxene, they have homogeneous chondritic Ni isotopic compositions which can be explained by meteoritic contamination (Fig. 5).

By contrast, lunar mare basalts have low Ni/Co ratios (<2, see compilation in Day, 2020), which are commonly thought to result from endogenous processes with none or negligible meteoritic contamination (Day, 2020; Ringwood and Seifert, 1986). Brenan et al. (2019) suggested that the lunar basalts can be universally contaminated with 0.01–1% of HSE-rich lunar megaregolith materials that contain impact debris, whereas Ni/Co is relatively insensitive to regolith contamination. Conversely, Day and Paquet (2021) suggested that the HSE systematics in mare basalts are inconsistent with assimilation of impact-contaminated regolith materials. Rather, they may be generated from residual metal- and sulfide-free sources (Day, 2018), and the variations in HESs are consistent with limited late accretion to the lunar mantle and crust (Day and Paquet, 2021). Studied lunar basalt meteorites have low Ni/Co ratios ranging from 0.9 to 2.4, which, according to both studies, likely suggests that they are of endogenous origin.

The studied lunar basalt meteorites have sub-chondritic $\delta^{60/58}$Ni values varying from +0.023‰ to +0.228‰. The Apollo lunar mare basalts analyzed by Saunders (2018) show even larger Ni isotopic variations (from −0.203‰ to +0.348‰). Lunar igneous differentiation is unlikely to explain the Ni isotopic variations in lunar basalts and the covariation between Ni/Co and $\delta^{60/58}$Ni. Olivine and pyroxene crystallization or accumulation can cause small variation in Ni/Co of the melts or cumulates, because both prefer Ni relative to Co during igneous processes. However, none of these can produce Ni isotope fractionations larger than ±0.05‰ (Sheng et al., 2022). And, if any, the melts would have lower Ni/Co and higher Ni isotope values, owing to the preference of heavy Ni isotopes in the melts relative to olivine and pyroxene (Klaver et al., 2022; Sheng et al., 2022). HSEs in sulfide and metal from mare basalts indicate removal of <0.1% of sulfide and metal during fractional crystallization of parental melts (Day and Paquet, 2021). Sulfide and metal are isotopically lighter and heavier, respectively, compared to the silicate (Fig. 3). The role of sulfide and metal separation on the Ni isotopic composition of lunar basaltic rocks needs further study. However, mass-balance calculation suggests that removal of <0.1% of either sulfide or metal cannot produce significant Ni isotopic variations in the evolved melts. A lack of correlation of Ni isotope value against sulfide or metal modal proportion in the Apollo samples may further support this idea (Saunders, 2018). Therefore, by analogy to the HEDs, the covariation of $\delta^{60/58}$Ni against Ni/Co in lunar samples indicate chondritic addition, likely achieved during the late accretion after core formation, and that the primitive silicate mantle of Moon is sub-chondritic in Ni isotopes. Nevertheless, placing a precise constraint on the average

Ni isotopic composition of the Bulk Silicate Moon (BSM) is challenging, not only because of the limited dataset of lunar basalts, but also the possibility of Ni isotopic heterogeneity of the lunar mantle.

4.4. Nickel isotopic perspective on the formation of Earth-Moon system

The lunar core takes up of only ~2% of the lunar total mass and the $D^{Ni}_{metal/silicate}$ is generally lower than 500 (Righter, 2011), which predicts that lunar core-forming process is unlikely to produce significant Ni isotope fractionation between core and mantle according to the mass balance model (Fig. 4). Therefore, it is likely that the bulk Moon is sub-chondritic in Ni isotopes. This has important implications on the Moon-forming giant impact as we will discuss.

According to the canonical model, the Moon-forming giant impact contributed ~10% of Earth's total mass (Canup and Asphaug, 2001). Prior to the giant impact, core-mantle differentiation in the proto-Earth occurred at high temperature of >2500 K and high pressures that correspond to $D^{Ni}_{metal\text{-}silicate}$ of <35 (Righter, 2011), leading to limited Ni isotope fractionations between silicate mantle and metallic core (Fig. 4). Given that the Earth accreted mainly from enstatite-like chondrites in the early accretion stages, the BSE of the proto-Earth is thought to have chondritic $\delta^{60/58}$Ni values.

However, the present BSE has a sub-chondritic δ^{60}Ni value of +0.10 ± 0.07‰ (Klaver et al., 2020; Wang et al., 2021). Due to the moderate siderophile nature, the Ni in the BSE was mostly derived from late-stage impactors, as that from earlier stages was largely segregated into the core (Dauphas, 2017). Therefore, Wang et al. (2021) proposed that this sub-chondritic Ni isotopic signature of the BSE was established during Earth's late stages of accretion. The Moon-forming impactor was the primary contributor of late-stage accretion additions to the Earth. According to the heterogeneous accretion model (Rubie et al., 2011; Zhou et al., 2022), the Moon-forming giant impact added >20% of the BSE's present Ni, while the following late veneer contributed <5% of the Ni budget of the BSE. Therefore, the Moon-forming impactor, Theia, was likely the major cause of the sub-chondritic Ni isotopic composition of BSE.

Our results of differentiated achondrites imply that core-mantle differentiation on small planetary bodies can potentially produce large Ni isotope fractionation, with the planetary mantle enriched in light Ni isotopes. Therefore, Theia was likely a differentiated planetary body with its mantle enriched in light Ni isotopes which were later introduced to the Earth's mantle via a core-merging giant impact (Wang et al., 2021; Zhou et al., 2022). Although both HEDs and highly reduced aubrites possess light Ni isotopic signatures (Fig. 1), the aubrite may provide the best candidate of meteorite analogy to the hypothesized Theia's mantle composition. Enstatite chondrite or enstatite chondrite-like differentiated planetary body are thought to be the main building blocks of the Earth, because of the similarities of nucleosynthetic isotopic compositions of a number of elements, including nickel (Dauphas, 2017). By contrast, other differentiated rocks from carbonaceous or ordinary chondrite-like parent bodies are characterized by different nucleosynthetic Ni isotopic compositions (Nanne et al., 2019; Wang et al., 2021). If Theia formed, differentiated and evolved under highly reduced conditions similar to that of AUPB or Mercury, it would have high sulfur and light Ni isotopic composition for its mantle.

We speculate that, following the main stages of Earth's accretion, the collision between the proto-Earth and a differentiated, Mars-sized impactor, yielded sub-chondritic Ni isotopic compositions for both BSE and BSM. Subsequent accretion of chondritic materials through late veneer has a limited effect on the Ni isotopic system of the BSE, but late accretion on the Moon have shifted the $\delta^{60/58}$Ni to chondritic value to various degrees. However, linking the nature of Theia and early formed small, differentiated planetary bodies to achondrite records can be obscured by late accretion, which was spatially and temporally widespread in the inner Solar System.

5. Conclusions

We measured the mass-dependent Ni isotopic compositions of a comprehensive set of achondrites and lunar rocks, and reached the following conclusions.

(1) The primitive achondrites display high Ni contents and invariant Ni isotopic compositions that fall within the chondritic range. Given incomplete core-mantle differentiation of primitive achondrite parent bodies, the chondritic Ni isotopic compositions are likely due to the retention of metal, which dominated the Ni budget and obscured any possible Ni isotope fractionation caused by metal-silicate-sulfide segregation processes.
(2) The differentiated achondrites show large Ni isotopic variations. The highly reduced aubrites and an ungrouped achondrite (NWA 8409) have the lowest $\delta^{60/58}$Ni values. Acid leaching experiments demonstrate that the sulfide fraction is a significant host of light Ni isotopes in aubrites. The most extreme Ni isotope values of aubrites may be due to large Ni isotope fractionation accompanied by silicate-sulfide-metal separation during differentiation of the parent bodies, and subsequent global disruptive collision and reassembly with variably high proportions of sulfides enriched in the mantle. The Ni isotopic compositions of the HEDs are positively correlated with the Ni/Co, which is caused by late accretion of chondritic materials after planetary core segregation. Thus, the pristine endmember of the HEDs has a sub-chondritic Ni isotopic composition, as a result of low-pressure and low-temperature core-mantle differentiation on their likely limited-sized parent body, Vesta.
(3) The lunar breccia meteorites have high Ni/Co ratios and homogenous chondritic Ni isotope values, which are thought to be caused impact contamination of chondritic debris. The mare basalt meteorites have lower Ni/Co ratios and are systematically isotopically lighter. The positive correlation between Ni isotope value and Ni/Co ratio indicates that late accretion on Moon can shift the $\delta^{60/58}$Ni approaching the chondritic value. Although the limited data set prevent us from placing a firm constraint on the average Ni isotopic composition of the BSM, it is likely sub-chondritic in Ni isotopes. We suggest that the Moon-forming impactor, Theia, was likely an aubrite-like differentiated planetary body whose mantle was enriched in light Ni isotopes.

Declaration of Competing Interest

The authors declare that they have no known competing financial interests or personal relationships that could have appeared to influence the work reported in this paper.

Acknowledgments

We thank Renbiao Tao for providing a lunar basalt meteorite. We also thank Frederic Moynier for his suggestions and efficient editorial handling, James Day, Stepan Chernonozhkin, and two anonymous reviewers for their helpful comments. This work was funded by the National Natural Science Foundation of China (Grants 41973010 and 42241103) to S.J.W. S.J.L was funded by the National Nature Science Foundation of China (Grant 42170346).

Appendix A. Supplementary material

Supplementary figures, including elemental constituents of a corroded diamond-coated wire, comparison of measured and certified Ni, Co and Fe/Ni of reference materials, Fe/Ni of studied achondrite samples, and Ni/Co ratio of metal grains in lunar breccias, can be found in the supplementary materials. Supplementary material to this article can be found online at https://doi.org/10.1016/j.gca.2023.04.004.

References

Archer, G.J., Walker, R.J., Irving, A.J., 2019. Highly siderophile element and 187Re-187Os isotopic systematics of ungrouped achondrite Northwest Africa 7325: Evidence for complex planetary processes. Meteorit. Planet. Sci. 54, 1042–1050.

Barrat, J.-A., Greenwood, R., Verchovsky, A., Gillet, P., Bollinger, C., Langlade, J., Liorzou, C., Franchi, I., 2015. Crustal differentiation in the early solar system: Clues from the unique achondrite Northwest Africa 7325 (NWA 7325). Geochim. Cosmochim. Acta 168, 280–292.

Beunon, H., Chernonozhkin, S.M., Mattielli, N., Goderis, S., Doucet, L.-S., Debaille, V., Vanhaecke, F., 2020. Innovative two-step isolation of Ni prior to stable isotope ratio measurements by MC-ICP-MS: application to igneous geological reference materials. J. Anal. At. Spectrom. 35, 2213–2223.

Bourdon, B., Roskosz, M., Hin, R.C., 2018. Isotope tracers of core formation. Earth-Sci. Rev. 181, 61–81.

Brenan, J.M., Mungall, J.E., Bennett, N.R., 2019. Abundance of highly siderophile elements in lunar basalts controlled by iron sulfide melt. Nat. Geosci. 12, 701–706.

Cameron, V., Vance, D., Archer, C., House, C.H., 2009. A biomarker based on the stable isotopes of nickel. Proc. Natl. Acad. Sci. U. S. A. 106, 10944–10948.

Campbell, A.J., Humayun, M., 2003. Formation of metal in Grosvenor Mountains 95551 and comparison to ordinary chondrites. Geochim. Cosmochim. Acta 67, 2481–2495.

Canup, R.M., Asphaug, E., 2001. Origin of the Moon in a giant impact near the end of the Earth's formation. Nature 412, 708–712.

Cartier, C., Charlier, B., Boyet, M., Spalding, C., Namur, O., 2022. A large proto-Mercury as the aubrite parent body. 53rd Lunar and Planetary Science Conference (2022) 163.

Casanova, I., Keil, K., Newsom, H.E., 1993. Composition of metal in aubrites: Constraints on core formation. Geochim. Cosmochim. Acta 57, 675–682.

Chernonozhkin, S.M., Goderis, S., Lobo, L., Claeys, P., Vanhaecke, F., 2015. Development of an isolation procedure and MC-ICP-MS measurement protocol for the study of stable isotope ratio variations of nickel. J. Anal. At. Spectrom. 30, 1518–1530.

Chernonozhkin, S.M., Goderis, S., Costas-Rodríguez, M., Claeys, P., Vanhaecke, F., 2016. Effect of parent body evolution on equilibrium and kinetic isotope fractionation: a combined Ni and Fe isotope study of iron and stony-iron meteorites. Geochim. Cosmochim. Acta 186, 168–188.

Cook, D.L., Leya, I., Schönbächler, M., 2020. Galactic cosmic ray effects on iron and nickel isotopes in iron meteorites. Meteorit. Planet. Sci. 55, 2758–2771.

Creech, J., Baker, J., Handler, M., Lorand, J.-P., Storey, M., Wainwright, A., Luguet, A., Moynier, F., Bizzarro, M., 2017a. Late accretion history of the terrestrial planets inferred from platinum stable isotopes. Geochem. Perspect. Lett 3, n1.

Creech, J., Moynier, F., Bizzarro, M., 2017b. Tracing metal–silicate segregation and late veneer in the Earth and the ureilite parent body with palladium stable isotopes. Geochim. Cosmochim. Acta 216, 28–41.

Dale, C.W., Burton, K.W., Greenwood, R.C., Gannoun, A., Wade, J., Wood, B.J., Pearson, D.G., 2012. Late accretion on the earliest planetesimals revealed by the highly siderophile elements. Science 336, 72–75.

Dauphas, N., 2017. The isotopic nature of the Earth's accreting material through time. Nature 541, 521.

Day, J.M.D., 2015. Planet formation processes revealed by meteorites. Geology Today 31, 12–20.

Day, J.M.D., 2018. Geochemical constraints on residual metal and sulfide in the sources of lunar mare basalts. Am. Mineral.: J. Earth Planet. Mater. 103, 1734–1740.

Day, J.M.D., 2020. Metal grains in lunar rocks as indicators of igneous and impact processes. Meteorit. Planet. Sci. 55.

Day, J.M.D., Paquet, M., 2021. Temporally limited late accretion after core formation in the Moon. Meteorit. Planet. Sci. 56, 683–699.

Day, J.M.D., Walker, R.J., Ash, R.D., Liu, Y., Rumble III, D., Irving, A.J., Goodrich, C.A., Tait, K., McDonough, W.F., Taylor, L.A., 2012a. Origin of felsic achondrites Graves Nunataks 06128 and 06129, and ultramafic brachinites and brachinite-like achondrites by partial melting of volatile-rich primitive parent bodies. Geochim. Cosmochim. Acta 81, 94–128.

Day, J.M.D., Walker, R.J., Qin, L., Rumble III, D., 2012b. Late accretion as a natural consequence of planetary growth. Nat. Geosci. 5, 614–617.

Dhaliwal, J.K., Day, J.M.D., Corder, C.A., Tait, K.T., Marti, K., Assayag, N., Cartigny, P., Rumble III, D., Taylor, L.A., 2017. Early metal-silicate differentiation during planetesimal formation revealed by acapulcoite and lodranite meteorites. Geochim. Cosmochim. Acta 216, 115–140.

Fischer, R.A., Nakajima, Y., Campbell, A.J., Frost, D.J., Harries, D., Langenhorst, F., Miyajima, N., Pollok, K., Rubie, D.C., 2015. High pressure metal–silicate partitioning of Ni Co, V, Cr, Si, and O. Geochim. Cosmochim. Acta 167, 177–194.

Fischer-Gödde, M., Becker, H., 2012. Osmium isotope and highly siderophile element constraints on ages and nature of meteoritic components in ancient lunar impact rocks. Geochim. Cosmochim. Acta 77, 135–156.

Gall, L., Williams, H.M., Halliday, A.N., Kerr, A.C., 2017. Nickel isotopic composition of the mantle. Geochim. Cosmochim. Acta 199, 196–209.

Ganguly, J., Domeneghetti, M.C., 1996. Cation ordering of orthopyroxenes from the Skaergaard intrusion: implications for the subsolidus cooling rates and permeabilities. Contrib. Mineral. Petrol. 122, 359–367.

Goodrich, C.A., 1992. Ureilites: A critical review. Meteoritics 27, 327–352.

Goodrich, C.A., Kita, N.T., Yin, Q.-Z., Sanborn, M.E., Williams, C.D., Nakashima, D., Lane, M.D., Boyle, S., 2017. Petrogenesis and provenance of ungrouped achondrite Northwest Africa 7325 from petrology, trace elements, oxygen, chromium and titanium isotopes, and mid-IR spectroscopy. Geochim. Cosmochim. Acta 203, 381–403.

Gueguen, B., Rouxel, O., Ponzevera, E., Bekker, A., Fouquet, Y., 2013. Nickel Isotope Variations in Terrestrial Silicate Rocks and Geological Reference Materials Measured by MC-ICP-MS. Geostand. Geoanal. Res. 37, 297–317.

Guignard, J., Quitté, G., Méheut, M., Toplis, M., Poitrasson, F., Connetable, D., Roskosz, M., 2020. Nickel isotope fractionation during metal-silicate differentiation of planetesimals: experimental petrology and ab initio calculations. Geochim. Cosmochim. Acta. 269, 238–256.

Hofmann, A., Bekker, A., Dirks, P., Gueguen, B., Rumble, D., Rouxel, O.J., 2014. Comparing orthomagmatic and hydrothermal mineralization models for komatiite-hosted nickel deposits in Zimbabwe using multiple-sulfur, iron, and nickel isotope data. Miner. Deposita 49, 75–100.

Hopp, T., Kleine, T., 2021. Ruthenium isotopic fractionation in primitive achondrites: Clues to the early stages of planetesimal melting. Geochim. Cosmochim. Acta 302, 46–60.

Horstmann, M., Humayun, M., Fischer-Gödde, M., Bischoff, A., Weyrauch, M., 2014. Si-bearing metal and niningerite in Almahata Sitta fine-grained ureilites and insights into the diversity of metal on the ureilite parent body. Meteorit. Planet. Sci. 49, 1948–1977.

Keil, K., 2010. Enstatite achondrite meteorites (aubrites) and the histories of their asteroidal parent bodies. Geochemistry 70, 295–317.

Keil, K., 2012. Angrites, a small but diverse suite of ancient, silica-undersaturated volcanic-plutonic mafic meteorites, and the history of their parent asteroid. Geochemistry 72, 191–218.

Keil, K., 2014. Brachinite meteorites: Partial melt residues from an FeO-rich asteroid. Geochemistry 74, 311–329.

Keil, K., McCoy, T.J., 2018. Acapulcoite-lodranite meteorites: Ultramafic asteroidal partial melt residues. Geochemistry 78, 153–203.

Keil, K., Ntaflos, T., Taylor, G., Brearley, A., Newsom, H., Romig Jr, A., 1989. The Shallowater aubrite: Evidence for origin by planetesimal impacts. Geochim. Cosmochim. Acta 53, 3291–3307.

Klaver, M., Ionov, D.A., Takazawa, E., Elliott, T., 2020. The non-chondritic Ni isotope composition of Earth's mantle. Geochim. Cosmochim. Acta 268, 405–421.

Klaver, M., Steenstra, E.S., Borchert, M., Welter, E., Wilke, M., Berndt, J., Klemme, S., 2022. The effect of alkalinity on NiO bond length in silicate glasses: Implications for Ni isotope geochemistry. Chem. Geol. 121070.

Kleine, T., Touboul, M., Bourdon, B., Nimmo, F., Mezger, K., Palme, H., Jacobsen, S.B., Yin, Q.-Z., Halliday, A.N., 2009. Hf–W chronology of the accretion and early evolution of asteroids and terrestrial planets. Geochim. Cosmochim. Acta 73, 5150–5188.

Koefoed, P., Amelin, Y., Yin, Q.-Z., Wimpenny, J., Sanborn, M.E., Iizuka, T., Irving, A.J., 2016. U-Pb and Al–Mg systematics of the ungrouped achondrite Northwest Africa 7325. Geochim. Cosmochim. Acta 183, 31–45.

Krott, A., Keil, K., Scott, E., Goodrich, C., Weisberg, M., 2014. Classification of meteorites and their genetic relationships. Treatise Geochem. 1, 1–63.

Lager, G., Meagher, E., 1978. High-temperature structural study of six olivines. Am. Mineral. 63, 365–377.

Lazar, C., Young, E.D., Manning, C.E., 2012. Experimental determination of equilibrium nickel isotope fractionation between metal and silicate from 500 C to 950 C. Geochim. Cosmochim. Acta 86, 276–295.

Li, S., Yin, Q.-Z., Bao, H., Sanborn, M.E., Irving, A., Ziegler, K., Agee, C., Marti, K., Miao, B., Li, X., 2018. Evidence for a multilayered internal structure of the chondritic acapulcoite-lodranite parent asteroid. Geochim. Cosmochim. Acta 242, 82–101.

Lin, Y., 2022. Enstatite chondrites: condensation and metamorphism under extremely reducing conditions and contributions to the Earth. Progress Earth Planet. Sci. 9, 1–16.

Liu, S., Li, Y., Ju, Y., Liu, J., Liu, J., Shi, Y., 2018. Equilibrium nickel isotope fractionation in nickel sulfide minerals. Geochim. Cosmochim. Acta 222, 1–16.

Luck, J.-M., Othman, D.B., Albarède, F., 2005. Zn and Cu isotopic variations in chondrites and iron meteorites: early solar nebula reservoirs and parent-body processes. Geochim. Cosmochim. Acta 69, 5351–5363.

McCoy, T.J., Carlson, W., Nittler, L., Stroud, R., Bogard, D., Garrison, D., 2006. Graves Nunataks 95209: A snapshot of metal segregation and core formation. Geochim. Cosmochim. Acta 70, 516–531.

McDonough, W.F., Sun, S.-S., 1995. The composition of the Earth. Chem. Geol. 120, 223–253.

Mezger, K., Schönbächler, M., Bouvier, A., 2020. Accretion of the Earth—Missing Components? Space Sci. Rev. 216, 1–24.

Mittlefehldt, D., 2014. Achondrites. Meteorit. Cosmochem. Process. 1, 235–266.

Mittlefehldt, D.W., 2015. Asteroid (4) Vesta: I. The howardite-eucrite-diogenite (HED) clan of meteorites. Geochemistry 75, 155–183.

Mittlefehldt, D.W., Bogard, D.D., Berkley, J.L., Garrison, D.H., 2003. Brachinites: Igneous rocks from a differentiated asteroid. Meteorit. Planet. Sci. 38, 1601–1625.

Mittlefehldt, D.W., McCoy, T.J., Goodrich, C.A., Kracher, A., 2018. Non-chondritic meteorites from asteroidal bodies. Planetary Materials. De Gruyter, pp. 523–718.

Moynier, F., Paniello, R.C., Gounelle, M., Albarède, F., Beck, P., Podosek, F., Zanda, B., 2011. Nature of volatile depletion and genetic relationships in enstatite chondrites and aubrites inferred from Zn isotopes. Geochim. Cosmochim. Acta 75, 297–307.

Moynier, F., Vance, D., Fujii, T., Savage, P., 2017. The isotope geochemistry of zinc and copper. Rev. Mineral. Geochem. 82, 543–600.

Namur, O., Charlier, B., Holtz, F., Cartier, C., McCammon, C., 2016. Sulfur solubility in reduced mafic silicate melts: Implications for the speciation and distribution of sulfur on Mercury. Earth Planet. Sci. Lett. 448, 102–114.

Nanne, J.A., Nimmo, F., Cuzzi, J.N., Kleine, T., 2019. Origin of the non-carbonaceous–carbonaceous meteorite dichotomy. Earth Planet. Sci. Lett. 511, 44–54.

Okada, A., Keil, K., Taylor, G.J., Newsom, H., 1988. Igneous history of the aubrite parent asteroid: Evidence from the Norton County enstatite achondrite. Meteoritics 23, 59–74.
Rankenburg, K., Humayun, M., Brandon, A., Herrin, J., 2008. Highly siderophile elements in ureilites. Geochim. Cosmochim. Acta 72, 4642–4659.
Ray, S., Garvie, L.A., Rai, V.K., Wadhwa, M., 2021. Correlated iron isotopes and silicon contents in aubrite metals reveal structure of their asteroidal parent body. Sci. Rep. 11, 1–13.
Render, J., Brennecka, G.A., Wang, S.-J., Wasylenki, L.E., Kleine, T., 2018. A distinct nucleosynthetic heritage for early solar system solids recorded by Ni isotope signatures. Astrophys. J. 862, 26.
Righter, K., 2011. Prediction of metal–silicate partition coefficients for siderophile elements: An update and assessment of PT conditions for metal–silicate equilibrium during accretion of the Earth. Earth Planet. Sci. Lett. 304, 158–167.
Righter, K., Drake, M.J., 1997. A magma ocean on Vesta: Core formation and petrogenesis of eucrites and diogenites. Meteorit. Planet. Sci. 32, 929–944.
Righter, K., Sutton, S.R., Danielson, L., Pando, K., Newville, M., 2016. Redox variations in the inner solar system with new constraints from vanadium XANES in spinels. Am. Mineral. 101, 1928–1942.
Ringwood, A., Seifert, S., 1986. Nickel-cobalt abundance systematics and their bearing on lunar origin, in Origin of the Moon, [Pap. Conf.], p. 249.
Rubie, D.C., Frost, D.J., Mann, U., Asahara, Y., Nimmo, F., Tsuno, K., Kegler, P., Holzheid, A., Palme, H., 2011. Heterogeneous accretion, composition and core–mantle differentiation of the Earth. Earth Planet. Sci. Lett. 301, 31–42.
Saunders, N., 2018. Nickel stable isotope fractionation in planetary materials. University of Oxford.
Saunders, N.J., Barling, J., Harvey, J., Halliday, A.N., 2020. Heterogeneous nickel isotopic compositions in the terrestrial mantle–Part 1: Ultramafic lithologies. Geochim. Cosmochim. Acta 285, 129–149.
Saunders, N.J., Barling, J., Harvey, J., Fitton, J.G., Halliday, A.N., 2022. Heterogeneous nickel isotope compositions of the terrestrial mantle–Part 2: Mafic lithologies. Geochim. Cosmochim. Acta 317, 349–364.
Sheng, S.Z., Wang, S.J., Yang, X.M., Chen, L.H., Zeng, G., Xiao, Y., Shen, J., Dong, X.H., Lv, Y.W., 2022. Sulfide dissolution on the nickel isotopic composition of basaltic rocks. J. Geophys. Res.: Solid Earth, e2022JB024555.
Spivak-Birndorf, L.J., Wang, S.-J., Bish, D.L., Wasylenki, L.E., 2018. Nickel isotope fractionation during continental weathering. Chem. Geol. 476, 316–326.
Steele, R.C., Elliott, T., Coath, C.D., Regelous, M., 2011. Confirmation of mass-independent Ni isotopic variability in iron meteorites. Geochim. Cosmochim. Acta 75, 7906–7925.
Tang, H., Dauphas, N., 2012. Abundance, distribution, and origin of 60Fe in the solar protoplanetary disk. Earth Planet. Sci. Lett. 359, 248–263.
Torigoye, N., Shima, M., 1993. Evidence for a late thermal event of unequilibrated enstatite chondrites: A Rb-Sr study of Qingzhen and Yamato 6901 (EH3) and Khairpur (EL6). Meteoritics 28, 515–527.
Unsalan, O., Jenniskens, P., Yin, Q.Z., Kaygisiz, E., Albers, J., Clark, D.L., Granvik, M., Demirkol, I., Erdogan, I.Y., Bengu, A.S., 2019. The Sariçiçek howardite fall in Turkey: Source crater of HED meteorites on Vesta and impact risk of Vestoids. Meteorit. Planet. Sci. 54, 953–1008.
van Acken, D., Brandon, A.D., Lapen, T.J., 2012. Highly siderophile element and osmium isotope evidence for postcore formation magmatic and impact processes on the aubrite parent body. Meteorit. Planet. Sci. 47, 1606–1623.
Wang, K., Day, J.M.D., Korotev, R.L., Zeigler, R.A., Moynier, F., 2014a. Iron isotope fractionation during sulfide-rich felsic partial melting in early planetesimals. Earth Planet. Sci. Lett. 392, 124–132.
Wang, S.-J., Rudnick, R.L., Gaschnig, R.M., Wang, H., Wasylenki, L.E., 2019. Methanogenesis sustained by sulfide weathering during the Great Oxidation Event. Nat. Geosci. 12, 296–300.
Wang, K., Savage, P.S., Moynier, F., 2014b. The iron isotope composition of enstatite meteorites: Implications for their origin and the metal/sulfide Fe isotopic fractionation factor. Geochim. Cosmochim. Acta 142, 149–165.
Wang, S.-J., Wang, W., Zhu, J.-M., Wu, Z., Liu, J., Han, G., Teng, F.-Z., Huang, S., Wu, H., Wang, Y., 2021. Nickel isotopic evidence for late-stage accretion of Mercury-like differentiated planetary embryos. Nat. Commun. 12, 1–7.
Weisberg, M.K., McCoy, T.J., Krot, A.N., 2006. Systematics and evaluation of meteorite classification. Meteorit. Early Sol. Syst. II 19, 19–52.
White, W.B., Mccarthy, G.J., Scheetz, B.E., 1971. Optical spectra of chromium, nickel, and cobalt-containing pyroxenes. Am. Mineral.: J. Earth Planet. Mater. 56, 72–89.
Wilbur, Z.E., Udry, A., McCubbin, F.M., Vander Kaaden, K.E., DeFelice, C., Ziegler, K., Ross, D.K., McCoy, T.J., Gross, J., Barnes, J.J., 2022. The effects of highly reduced magmatism revealed through aubrites. Meteorit. Planet. Sci. 57, 1387–1420.
Yang, J., Lin, Y., Changela, H., Xie, L., Chen, B., Yang, J., 2020. Early sulfur-rich magmatism on the ungrouped achondrite Northwest Africa 7325 differentiated parent body. Meteorit. Planet. Sci. 55, 1951–1978.
Zhou, Y., Liu, Y., Reinhardt, C., Deng, H., 2022. The core-merging giant impact in Earth's accretion history and its implications. Acta Geochim. 41, 553–567.
Zhu, K., Moynier, F., Alexander, C.M.D., Davidson, J., Schrader, D.L., Zhu, J.-M., Wu, G.-L., Schiller, M., Bizzarro, M., Becker, H., 2021a. Chromium stable isotope panorama of chondrites and implications for Earth early accretion. Astrophys. J. 923, 94.
Zhu, K., Moynier, F., Schiller, M., Becker, H., Barrat, J.-A., Bizzarro, M., 2021b. Tracing the origin and core formation of the enstatite achondrite parent bodies using Cr isotopes. Geochim. Cosmochim. Acta 308, 256–272.
Zhu, K., Barrat, J.A., Yamaguchi, A., Rouxel, O., Germain, Y., Langlade, J., Moynier, F., 2022. Nickel and chromium stable isotopic composition of ureilites: Implications for the Earth's core formation and differentiation of the ureilite parent body. Geophys. Res. Lett. 49, e2021GL095557.
Zhu, K., Becker, H., Zhu, J.-M., Xu, H.-P., Man, Q.-R., 2023. Planetary accretion and core formation inferred from Ni isotopes in enstatite meteorites. Geochem. Perspect. Lett 25, 1–7.